

## Research Article

# Graphene Oxide Films Obtained by Vacuum Filtration: X-Ray Diffraction Evidence of Crystalline Reorganization

Julia L. S. Gascho , Sara F. Costa , Abel A. C. Recco , and Sérgio H. Pezzin 

Graduate Program in Materials Science and Engineering, Center of Technological Sciences, Santa Catarina State University, Joinville, SC 89.219-710, Brazil

Correspondence should be addressed to Sérgio H. Pezzin; [sergio.pezzin@udesc.br](mailto:sergio.pezzin@udesc.br)

Received 7 April 2018; Revised 5 December 2018; Accepted 12 December 2018; Published 24 March 2019

Academic Editor: Xuping Sun

Copyright © 2019 Julia L. S. Gascho et al. This is an open access article distributed under the Creative Commons Attribution License, which permits unrestricted use, distribution, and reproduction in any medium, provided the original work is properly cited.

In this study, films of graphene oxide and chemically or thermally reduced graphene oxide were produced by a simple vacuum filtration method and submitted to a thorough characterization by X-ray diffraction (XRD), Raman and infrared spectroscopies, field-emission scanning electron microscopy, transmission electron microscopy, atomic force microscopy, confocal microscopy, and contact angle measurements. Graphene oxide (GO) was produced from graphite by the modified Hummers method and thereafter reduced with  $\text{NaBH}_4$  or by heating under argon in a tubular furnace. The films were produced from aqueous solutions by vacuum filtration on a cellulose membrane. Graphite presents two characteristic XRD peaks corresponding to  $d = 0.34$  nm and  $d = 0.17$  nm. After oxidation, only a peak at  $d = 0.84$  nm is found for powder GO, confirming the insertion of oxygen groups with an increase in the interplanar distance of graphene nanoplatelets. However, for GO films, other unexpected peaks are observed at  $d = 0.63$  nm,  $d = 0.52$  nm, and  $d = 0.48$  nm. After reduction, both chemical and thermal, the peak at 0.84 nm disappears, while those corresponding to interplanar distances of 0.63 nm, 0.52 nm, and 0.48 nm are still present. The other characterizations confirm the production and chemical composition of GO and reduced GO films. The results indicate the combination of crystalline regions with different interplanar distances, suggesting the ordering of graphene/graphene oxide intercalated sheets.

## 1. Introduction

Graphene can be obtained by various methods, such as mechanical exfoliation, chemical vapor deposition phase, and also oxidation of graphite, which is abundant and has low cost, one of the reasons for this being one of the most used methods [1–6]. Graphene oxide (GO) consists of two-dimensional (2D) sheets of covalently linked carbon atoms, i.e., graphene sheets, presenting oxygenated functional groups such as hydroxyl, carbonyl, and epoxy, in its basal planes and edges [5, 7, 8]. The presence of these oxygenated groups between the graphene sheets generates substantial insulating domains, due to the presence of carbon atoms with  $\text{sp}^3$  hybridization which interrupts the passage of electrons between the planar carbons ( $\text{sp}^2$ ) [9]. Nevertheless, these groups can be further eliminated by reduction

reactions, producing reduced graphene oxide (RGO) or graphene, in the case of a single nanoplatelet [7, 10].

Graphene's structure and performance advantages, such as a high surface-to-volume ratio and high charge mobility, can be translated into highly sensitive sensing applications. Graphene and GO and RGO films have been recently extensively studied because of their applications in electronics [11, 12]. These films have become exciting new materials for the design of novel devices and sensing platforms in fields spanning from electronics to chemistry and biomedical applications. A graphene film has been shown to be a promising candidate for ITO replacement as conductive and transparent electrodes [13–15]. Conductive and transparent RGO films, capable of being used as electrodes, have already been produced, however, by methods different from those proposed in this work [1, 12–16].

X-ray diffraction (XRD) has been used to study the morphology of nanostructured materials such as graphene, where carbon atoms are linked to form atomic planes, also called nanoplatelets or lamellae, present in the material. Graphite has two characteristic peaks at  $2\theta = 26^\circ$  ( $d = 0.34$  nm) and  $2\theta = 55^\circ$  ( $d = 0.17$  nm). After oxidation, forming graphene oxide, these peaks are shifted to smaller angles, while other peaks may appear in XRD analyses after the formation of GO films [17, 18]. For instance, Brahmayya et al. in 2017 used a simple procedure to prepare a nanomaterial by grafting sulfonated phenyl radicals on the reduced GO surface under irradiation with ultrasound, and they obtained an XRD spectrum that is not commonly found in the literature for this type of graphitic material [19]. Hiramatsu et al. in 2013 also found unusual XRD peaks for graphene nanowalls produced by plasma-enhanced chemical vapor deposition [20]. An unusual XRD peak, at about  $17^\circ$ , was also observed by Lu et al. in 2017 for graphene/GO films produced by a simple vacuum filtration method [21].

In this work, graphene oxide (GO) and reduced graphene oxide (RGO) films were produced through a simple and low-cost filtration method, assessing the efficiency of the methods of graphite oxidation, GO reduction, and film production. GO was produced from graphite by the modified Hummers method and further chemically reduced with  $\text{NaBH}_4$  or thermally reduced in a tubular oven. The samples were characterized by X-ray diffraction (XRD), Raman spectroscopy, Fourier transform infrared spectroscopy (FTIR), field effect scanning electron microscopy (FEG/SEM), transmission electron microscopy (TEM), atomic force microscopy (AFM), and confocal microscopy. The samples were then compared with those found in the literature, checking for the distinctive properties of the produced GO and RGO films.

## 2. Materials and Methods

**2.1. Graphite Oxidation.** Graphene oxide (GO) was produced using the Hummers method from natural graphite provided by *Graphite of Brasil*. Process times and proportions of the reagents were modified as suggested by Hirata et al. in 2004 [3, 22].

**2.2. Preparation of GO Films.** GO was dispersed in deionized water via sonication (Sonics VCX 750), and the GO films were prepared by vacuum filtration on a cellulose membrane ( $0.45 \mu\text{m}$ ). For the production of the films, 10 mL of each solution was filtered. In the production of GOF, a GO solution of 3 mg/mL was used, producing a film with about 3 mg of GO.

**2.3. Production of Reduced Graphene Oxide (RGO) Films by Chemical Reduction.** About 50 mg of GO was dispersed in 50 mL of deionized water by sonication (Sonics VCX 750). The solution was vacuum filtered ( $26 \text{ L/s}\cdot\text{m}^2$ ) and heated to  $80^\circ\text{C}$  under magnetic stirring, with the subsequent addition of 10 mL of a 4%  $\text{NaBH}_4$  solution, previously prepared, as the reducing agent. The mixture was maintained at  $80^\circ\text{C}$  under magnetic stirring for 1 hour after the addition of the reducing agent. The solution was subjected to normal

filtration ( $26 \text{ L/s}\cdot\text{m}^2$ ) and washed with deionized water until reaching a pH close to 7. The material retained on the filter paper was dispersed in deionized water by sonication (Sonics VCX 750). The dispersion was vacuum filtered ( $55 \text{ L/s}\cdot\text{m}^2$ ), giving origin to the RGO solution for the production of the films. From this RGO solution, an amount of 0.1 mg/mL was made, of which 10 mL was filtered on a cellulose membrane ( $0.45 \mu\text{m}$ ) forming the chemically reduced GO film (CGOF).

**2.4. Production of RGO Films by Thermal Reduction.** GO films were prepared as previously described and treated in an AN1031/Eurotherm 2416 tubular oven under an argon atmosphere (with a gas flow of one bubble per second). The GOF were heated from  $20^\circ\text{C}$  to  $800^\circ\text{C}$  at  $5^\circ\text{C}/\text{minute}$ , and heating was switched off immediately after the oven temperature reached  $800^\circ\text{C}$  producing thermally reduced GO films (TGOF).

**2.5. Characterization.** In order to determine the interplanar spacing of the atomic planes present in the material, the X-ray diffraction (XRD) technique (Shimadzu XRD 6000) was used, with a  $2\theta$  angle ranging from  $5$  to  $70^\circ$  and a wavelength of  $1.5406 \text{ \AA}$ , at 40 kV and 30 mA. All samples were measured on an amorphous silicon sample holder.

Raman spectroscopy analyses were performed in LabRAM equipment (Horiba Jobin Yvon). The spectra were obtained using a potency of approximately  $0.5 \text{ mW}$ , acquisition time of 60 seconds, from  $100$  to  $3600 \text{ cm}^{-1}$ , 4 accumulations, and a He-Ne laser ( $632.8 \text{ nm}$ ). Six different points of each sample were analyzed.

FTIR analyses were performed in a Spectrum One B spectrometer (PerkinElmer) by specular reflectance with a fixed angle, with 16 scans in the spectral region of  $4000$  to  $450 \text{ cm}^{-1}$ , and using a resolution of  $4 \text{ cm}^{-1}$ .

Field effect scanning electron microscopy (FE-SEM, JEOL JSM-6701F) was used to evaluate the morphology of the GO and RGO films. Optical images were captured through a DCM-FZ150 Panasonic camera in order to verify the translucency of the samples, i.e., the possibility of looking through the produced films, as well as to verify other characteristics visible to the naked eye.

Transmission electron microscopy (TEM) and selected-area electron diffraction (SAED) patterns were performed in JEOL JEM-2100 equipment. For the analyses, the samples were placed on a TEM grid and attached to the equipment holder. The films were analyzed by plain view, i.e., orienting the specimen surface perpendicular to the electron beam.

Atomic force microscopy (AFM) Nanite B (NanoSurface) was used to image the surface topography. AFM micrographs were obtained by scanning a  $5 \mu\text{m} \times 5 \mu\text{m}$  area with 256 scanned points per line, at 1 scanned line per second. Both  $x$ -axis and  $y$ -axis scans were identical. Scans were carried out in noncontact mode.

The thickness of graphene oxide and reduced graphene oxide films was estimated by 3D images taken on a Leica DCM 3D confocal microscope.

Contact angles were measured in a KSV optical tensiometer, model CAM 101. The following liquids were used: deionized water for 31 images and chloroform for 5 images.

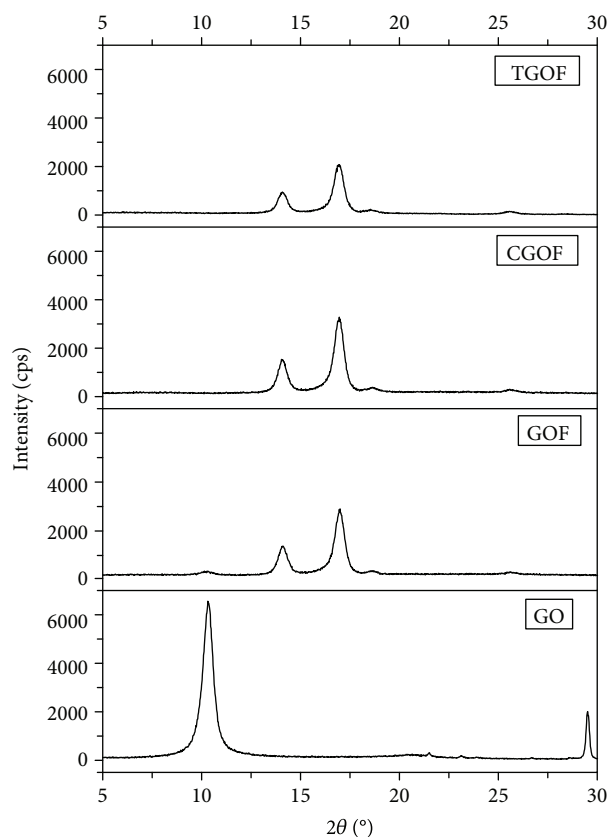


FIGURE 1: X-ray diffractograms of powder graphene oxide (GO), graphene oxide film (GOF), chemically reduced graphene oxide film (CGOF), and thermally reduced graphene oxide film (TGOF).

The images obtained were analyzed by the software “Attention Theta.” From the contact angle of the liquids with the samples, the surface tension of the films was calculated. Measurements of the contact angles were carried out with water ( $\gamma_L = 72.8 \text{ mJ/m}^2$ ,  $\gamma_L^d = 21.8 \text{ mJ/m}^2$ , and  $\gamma_L^p = 51.0 \text{ mJ/m}^2$ ) [23] and with chloroform ( $\gamma_L = 27.5 \text{ mJ/m}^2$ ,  $\gamma_L^d = 27.5 \text{ mJ/m}^2$ , and  $\gamma_L^p = 0 \text{ mJ/m}^2$ ) [24] in order to determine the surface tension of the analyzed solid through equations. The data was treated by the Owens-Wendt method.

### 3. Results and Discussion

**3.1. X-Ray Diffraction (XRD).** The X-ray diffractogram for graphite provided two characteristic peaks of this material at  $2\theta = 26^\circ$  ( $d_{002} = 0.34 \text{ nm}$ ) and  $2\theta = 55^\circ$  ( $d_{004} = 0.17 \text{ nm}$ ), corresponding to planes (002) and (004), respectively [6, 25].

After oxidation, these peaks are shifted to smaller angles. In the X-ray diffractogram of the GO (Figure 1), only a 002 peak at  $2\theta = 10^\circ$  ( $d_{002} = 0.84 \text{ nm}$ ) is found, confirming the efficiency of the oxidation reaction with an increase in the interplanar distance of the graphene nanoplatelets due to the insertion of oxygen groups [17, 19, 26, 27]. However, after the formation of GO films, other peaks are observed at  $2\theta = 14^\circ$  ( $d_{002} = 0.63 \text{ nm}$ ),  $2\theta = 17^\circ$  ( $d_{002} = 0.52 \text{ nm}$ ), and  $2\theta = 19^\circ$  ( $d_{002} = 0.48 \text{ nm}$ ), which were not yet reported in the

literature for this type of material, as well as a low-intensity peak at  $2\theta = 26^\circ$  ( $d_{002} = 0.34 \text{ nm}$ ), referring to graphite.

After chemical or thermal reduction, the GO films presented X-ray diffractograms without the presence of the peak at  $2\theta = 10^\circ$  (Figure 1), while the peaks at  $2\theta = 14^\circ$  ( $d_{002} = 0.63 \text{ nm}$ ),  $2\theta = 17^\circ$  ( $d_{002} = 0.52 \text{ nm}$ ), and  $2\theta = 19^\circ$  ( $d_{002} = 0.48 \text{ nm}$ ) continue to appear even after reduction. This indicates a partial reduction of the GO, as it was verified in the FTIR characterization.

The peak at  $2\theta = 10^\circ$  was already expected for the GO, due to the increase in the interplanar distance between the nanoplatelets after the insertion of the oxygenated groups, as well as the peak at  $2\theta = 26^\circ$  with low intensity, referring to some remaining graphite platelets. It must be highlighted that the XRD diagram for powder GO is different from that presented for the GOF, with the appearance of new peaks representing interplanar distances smaller than  $0.84 \text{ nm}$ . This can be attributed to the vacuum filtration process, which probably causes a partial restacking of the sheets of graphene and graphene oxide in the material.

The relatively sharp peak at  $2\theta = 14^\circ$  has not yet been observed for this type of material, although Brahmayya et al. have found a peak for GO close to it at  $2\theta = 12.8^\circ$  ( $d = 0.69 \text{ nm}$ ). After the chemical reduction of exfoliated graphene oxide with sodium borohydride and subsequent grafting of sulfonic acid containing aromatic radicals, this peak has been shifted to  $2\theta = 26.5^\circ$  ( $d = 0.34 \text{ nm}$ ), which they attributed to a  $\pi$ - $\pi$  restacking of the sulfonated RGO nanosheets [19]. A peak close to  $19^\circ$  was also observed by Arbutov et al. for GO reduced with hydrazine or by heating, but it was not so sharp and defined like those obtained in this work [6].

Other works using vacuum filtration to produce GO films [20, 26, 27] attributed the peak at  $26^\circ$  to the  $\pi$ - $\pi$  restacking of graphene sheets. Recently, Lu et al. [21] obtained graphene/GO films through a vacuum filtration method similar to the one used in this work, reporting an XRD peak close to  $17^\circ$ , suggesting that the GO sheets were uniformly dispersed between the sheets of graphene, i.e., a film of graphene intercalated with GO sheets [20].

To avoid the restacking of graphene sheets, several researchers have been proposing the insertion of spacers between them, such as liquid electrolytes, carbon nanotubes, polymers, nanoparticles, water, graphene balls, and fullerene. However, because of the weak interaction between these spacers and the graphene sheets, these films will have low capacitance, which explains the difficulty of obtaining highly conductive graphene films by simple filtration methods [27–29].

**3.2. Raman Spectroscopy.** Raman spectra for the GO film (GOF), chemically reduced GO film (CGOF), and thermally reduced GO film (TGOF) are shown in Figure 2.

Table 1 shows relevant data of Raman characterization, such as the wavenumbers of D and G peaks and  $I_D/I_G$  ratios.

The most prominent feature in the graphite spectrum is an acute G peak at around  $1583 \text{ cm}^{-1}$  corresponding to the vibrations in the graphite structure plane and a peak at around  $1370 \text{ cm}^{-1}$  corresponding to the disorder band, D [30]. In the spectra of the films obtained in this work, we can see the presence of wide D and G bands, not so

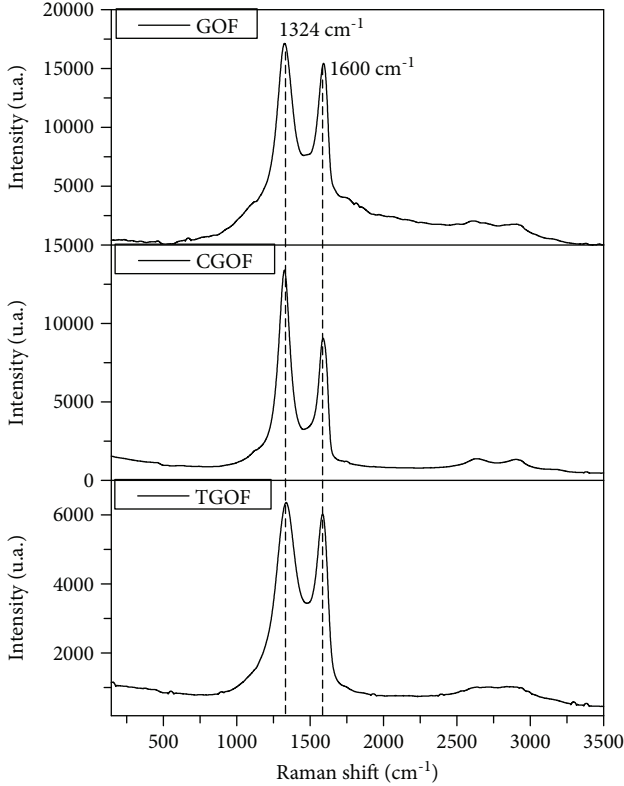


FIGURE 2: Raman spectra of graphene oxide film (GOF), chemically reduced graphene oxide film (CGOF), and thermally reduced graphene oxide film (TGOF).

TABLE 1: Raman spectroscopy.

Sample	$D$ peak ( $\text{cm}^{-1}$ )	$G$ peak ( $\text{cm}^{-1}$ )	$I_D/I_G$ ratio
GOF	1332	1592	0.83
CGOF	1327	1588	1.65
TGOF	1338	1588	1.55

well resolved as for graphite. In the case of the GO film, this could be related to the insertion of functional groups during the oxidation of graphite, which increases the topological disorder of the material. Nevertheless, this behavior remains for the reduced GO films (CGOF and TGOF), indicating that this type of structure has not changed.

$I_D/I_G$  ratios can be determined by the heights or areas of the peaks. Some groups use the Lorentzian function to calculate the ratio using the peak intensities, while others use the Gaussian function to make the relation between peak areas. According to Ferrari and Robertson, the difference is not so important for the disordered graphite because the peak widths are similar; however, it is important for amorphous carbon. In the latter case, the widening of the peak  $D$  is related to a distribution of agglomerates with different orders and dimensions; thus, the information about the

aromatic rings is less distorted in the maximum intensity than in the width, which depends on the disorder [31]. In this work, the values of the  $I_D/I_G$  ratios were calculated using the area of the peaks.

GO films presented the lowest  $I_D/I_G$  ratio, while higher ratios were found for the reduced GO films. It is also noteworthy that CGOF and TGOF presented close  $I_D/I_G$  ratios.

The  $I_D/I_G$  ratio is a measure of the degree of disorder and is inversely proportional to the mean size of the  $\text{sp}^2$  clusters present in the material. Thus, in carbon materials, the higher the  $I_D/I_G$  ratio, the greater the structural disorder. The GO reduction process can be expressed in Raman spectra by changes in the relative intensity of the  $D$  and  $G$  bands. As already mentioned, the  $I_D/I_G$  ratios are higher for the reduced GO films (CGOF and TGOF), which suggests that new (or more) graphite domains are formed and the number of  $\text{sp}^2$  clusters is increased during the reduction. This indicates an efficient reduction, corroborating with the results obtained by the surface energy characterizations. Similar results were obtained by Fim [32].

Besides the bands  $D$  and  $G$ , there are two Raman bands with weaker intensity, called  $2D$  and  $D+G$ , located between approximately  $2700$  and  $3000 \text{ cm}^{-1}$ . The  $2D$  band is present in Raman spectra for crystalline graphite materials and is sensitive to the  $\pi$  band in the graphitic electronic structure, while the  $D+G$  combination mode is induced by the disorder. The  $2D$  and  $D+G$  bands are usually ignored in the GO and RGO studies due to the low intensity of these bands in the Raman spectra for these materials. This was also noted in the present work, as observed in Figure 2 [33].

The  $2D$  band is considered the second order of the  $D$  band resulting from a two-cell vibrational process [20], and it is used to determine the thickness of the graphene layer. In contrast to the  $G$  band position method, the  $2D$  band method depends not only on the position of the band but also on the shape of the band. The  $D$  peak for graphene is a single sharp peak with a full width at half maximum (FWHM) of about  $30 \text{ cm}^{-1}$ , while in graphite it is a band consisting of more peaks. Thus, for more than 5 layers of graphene, the Raman spectrum becomes hardly distinguishable from that of bulky graphite.

As the number of graphene layers increases, the intensity of the  $2D$  band tends to decrease while that of the  $G$  band increases significantly. According to Kaniyoor and Ramaprabhu in 2012, the  $2D$  band in graphite maintains a profile of two peaks with the presence of up to 5 or 6 layers of graphene. However, in samples with high disorder, the two-peak profile of graphite is not maintained. Nevertheless, for a sample to be identified as a single graphene layer along with the single peak nature of the  $2D$  band, its intensity must be greater than that of the  $G$  band [34].

Thus, from the Raman spectra shown in Figure 3, we can identify that due to the lower intensity of the  $2D$  band in relation to the  $G$  band peak and due to their shape, which maintains a two-peak profile, the films have multiple layers of graphene, i.e., more than of six stacked graphene layers.

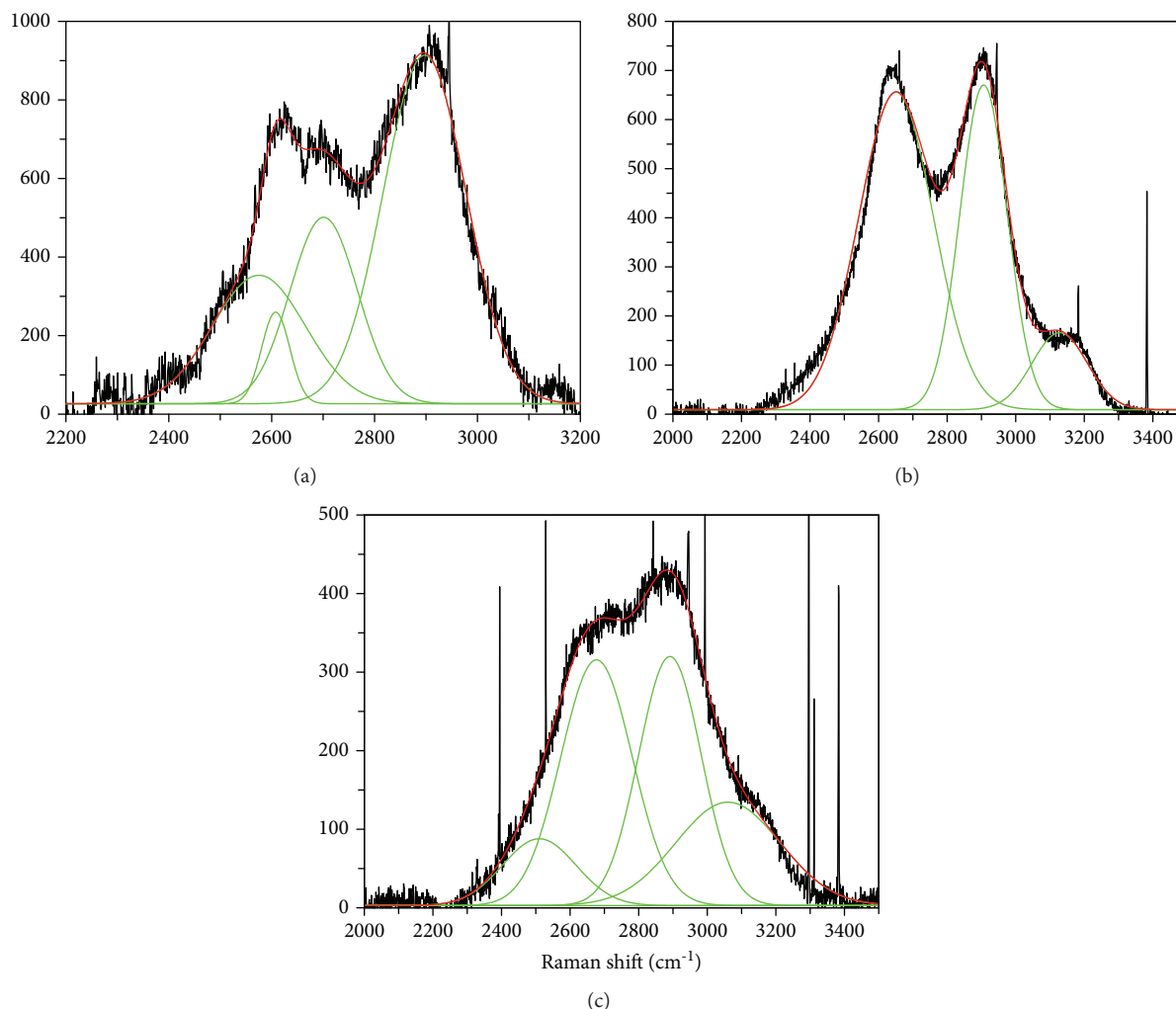


FIGURE 3: Raman spectra for the 2D region of the GOF, CGOF, and TGOF films.

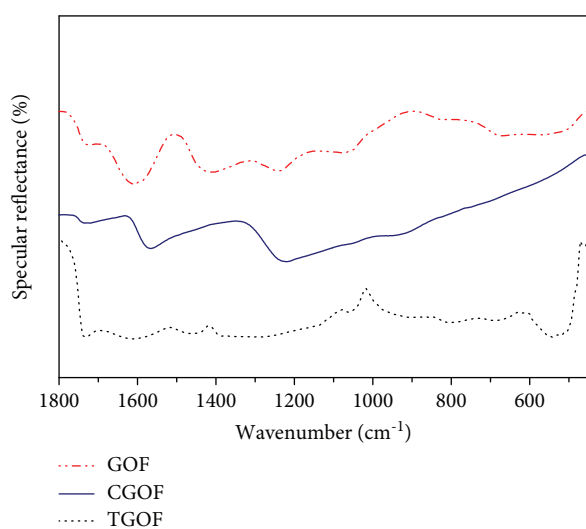


FIGURE 4: FTIR spectra for GOF, CGOF, and TGOF samples.

Nevertheless, graphitic materials with the same crystalline structure of the films produced in this work have not yet been reported in the literature. The XRD results indicate that the GO and RGO films produced in this work have a distinct crystalline structure with different interplanar distances, suggesting that the combination of graphene and GO sheets (intercalated) forms new crystalline domains.

**3.3. Fourier Transform Infrared Spectroscopy (FTIR).** Figure 4 shows the FTIR spectra for the GOF, CGOF, and TGOF samples. The GOF spectrum presented in Figure 3 indicates the oxidation of graphite, due to the presence of characteristic bands related to oxygenated groups [11, 35–41].

FTIR analyses performed on CGOF and TGOF indicate the partial reduction of GO (CGOF and TGOF curves), as some bands disappeared and others significantly decreased their intensity, both results corroborating with what was observed by the other characterizations previously presented.

The bands at 1730, 1600, and 1240  $\text{cm}^{-1}$  presented in the GOF spectrum are related to the axial deformation of the C=O bond, to the axial deformation of the C=C aromatic

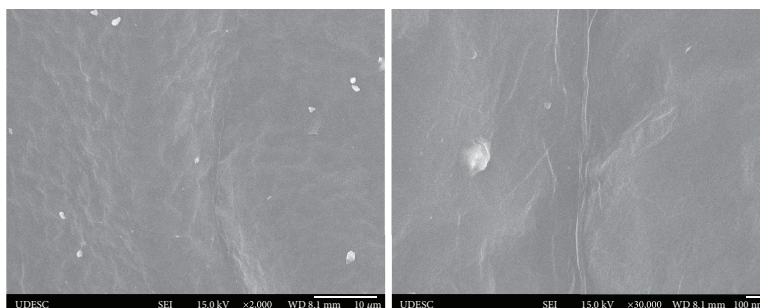


FIGURE 5: FE-SEM images of the surface of graphene oxide films.

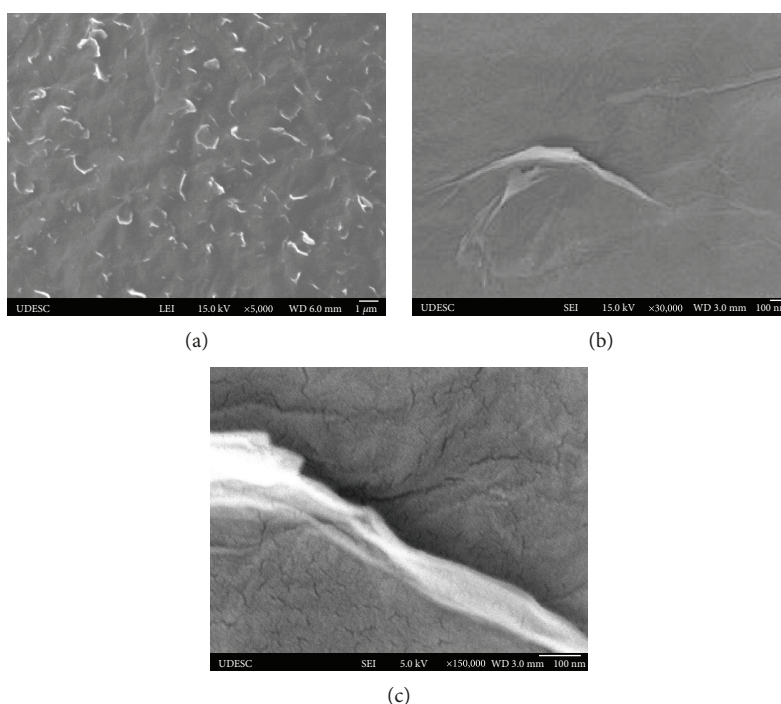


FIGURE 6: FE-SEM images of the surface of chemically reduced graphene oxide films.

bond, and to the asymmetric axial deformation of the COC bond, respectively. These bands are also present in the spectra of the CGOF and TGOF, but with a lower intensity.

The band relative to the stretching of the C-O bond in the  $1080\text{ cm}^{-1}$  region, present in the GOF spectrum, has practically disappeared through the two types of reduction, although it can be detected in the CGOF sample spectrum at a minimum amount. The band in the  $600\text{ cm}^{-1}$  region present in the GOF spectrum, concerning the deformation of the aliphatic C-H bond, also appears in the spectrum of the TGOF film at a very small intensity.

**3.4. Field Emission Gun Scanning Electron Microscopy (FE-SEM).** Field emission gun scanning electron microscopy (FE-SEM) analysis was used to verify the morphology of the films produced in this work. Figure 5 presents images of the GOF sample. In the images, it is observed that the film is flat with an almost one-dimensional fold and a scale of length

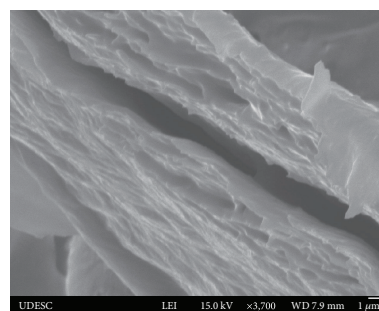


FIGURE 7: FE-SEM image of the transversal section of chemically reduced graphene oxide films.

between 3 and  $10\ \mu\text{m}$ . These folds are probably derived from the overlap of graphene nanoplatelets, where some edges of these nanoplatelets curl or bend during the formation of the GO film. Wang et al. [40] and Feng et al. [41] obtained

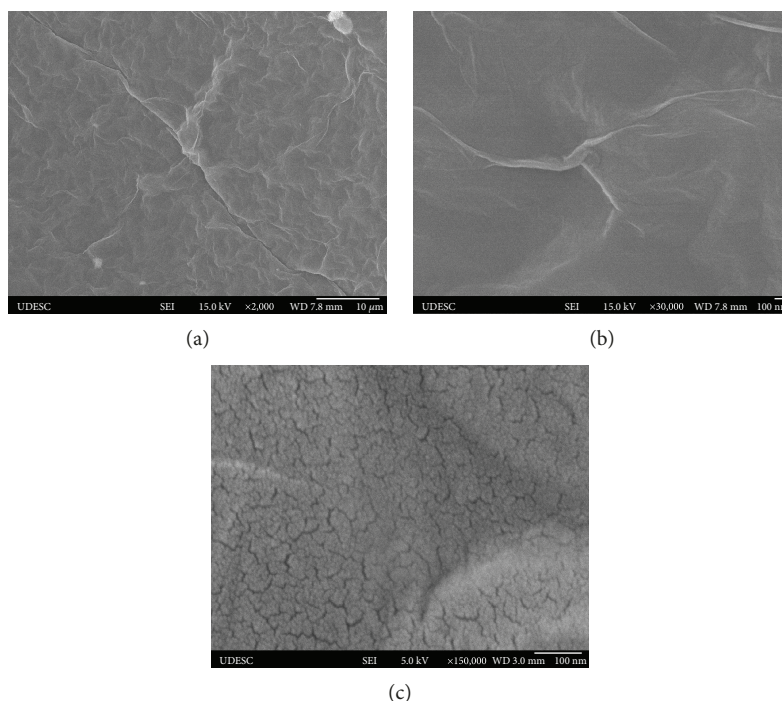


FIGURE 8: FE-SEM images of the surface of thermally reduced graphene oxide films.

similar results for GO films. They used the same method used in this work to produce GO, but the films were prepared by dip coating.

Figure 6 shows the images obtained by FEG/SEM for a chemically reduced GO film (CGOF), where the folds pertaining to the stacking of the graphene nanoplatelets can be seen, as well as the edges of some superimposed nanoplatelets. It is also possible to observe the contour of graphene nanoplatelets (Figure 6(c)). Wan et al. [37] produced reduced GO films with aluminum and obtained similar FEG images, although with a greater number of folds. Nekahi et al. [14] and Bora et al. [42] also reported similar results using hydroiodic acid and hydrazine, respectively, for the chemical reduction of the GO.

In addition, images of the CGOF sample were obtained in the transversal position (Figure 7), where it is possible to observe the spacing between the graphene nanoplatelets and the exfoliated aspect of the film. Other researchers obtained similar images for RGO films produced by other methods [6, 14, 15].

The images obtained for the thermally reduced GO film (TGOF), are presented in Figure 8 and were similar to those obtained for the GO films, only with a larger number of folds coming from the overlap of the graphene nanoplatelets.

The contour of the graphene nanoplatelets is verified in images with larger increases (Figure 6(c)). Hun [43] and Wan et al. [37] obtained films with similar characteristics, observing an almost one-dimensional fold coming from the overlap of graphene nanoplatelets. Moreover, they obtained films with an irregular surface, similar to those that occurred for the thermally reduced GO films reported here,

which did not present a flat surface like GO films and chemically reduced GO films. This wrinkled morphology can enhance the use of these films in catalysis, as the substrates can easily access the active sites on both side surfaces of the 2D graphene nanosheets [19].

In the images of Figures 6(c) and 8(a), the edges of some nanoplatelets stand out, indicating the reduction of GO. In addition, the folding of graphene sheets was also noted.

**3.5. Transmission Electron Microscopy (TEM).** TEM images of graphene oxide films are shown in Figures 9(a)–9(c). It is observed that GOF is basically transparent and that the curled or folded edges usually result in different levels of brightness in the image [44, 45]. In the SAED pattern (Figure 10(d)), clear diffraction spots are observed, characteristic of crystalline order and preferential crystalline orientation. This image illustrates a symmetrical six-fold pattern with the corresponding Miller-Bravais indices, which refers to graphite/graphene [19, 45, 46]. The circle and the more discrete bright spots indicate that the analyzed material does have a significant number of superimposed sheets [46, 47]. The characterization of isolated GO nanoplatelets produced in our laboratory can be found elsewhere [47].

**3.6. Atomic Force Microscopy (AFM).** AFM analysis has been used for determining the thickness of the flakes of layered 2D materials [33]. In the AFM image (Figure 10(a)), it is possible to identify the contours of a graphene nanoplatelet, highlighted within the blue square. Thus, the distribution of the flake thickness was obtained by measuring the height of

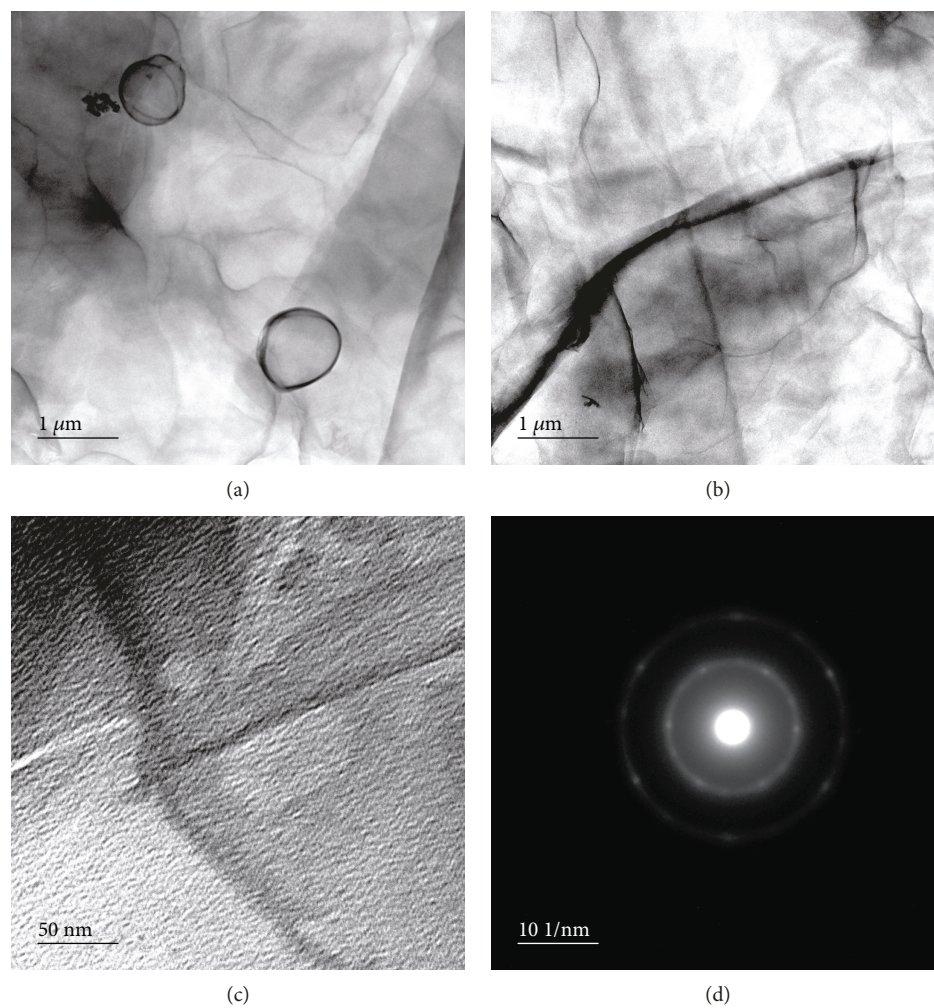


FIGURE 9: TEM images of graphene oxide films (GOF): (a) a flat surface; (b) crumpled surface; (c) higher magnification image of a GOF stepped surface; (d) SAED pattern.

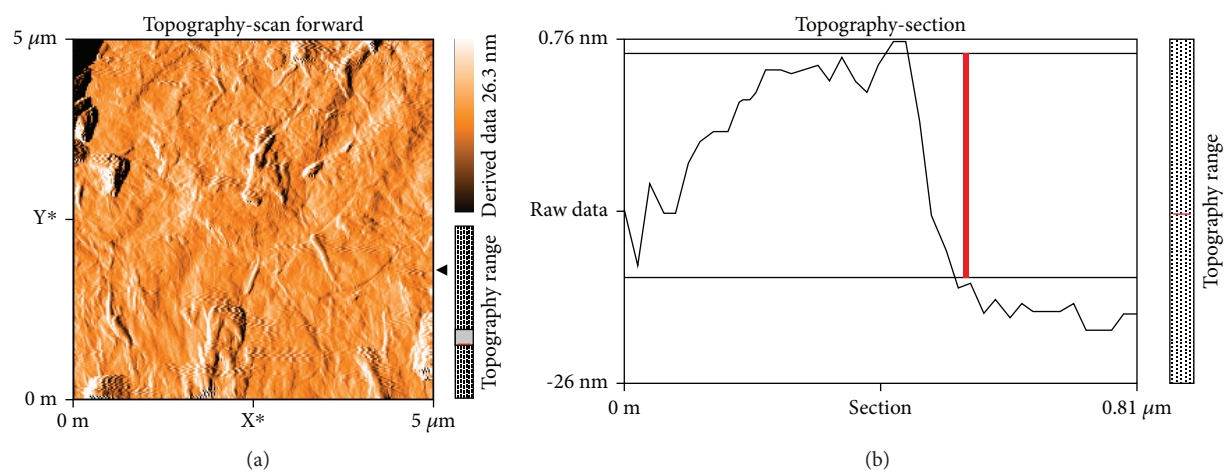


FIGURE 10: Atomic force microscopy (AFM) for CGOF: (a) AFM image and (b) AFM profile.

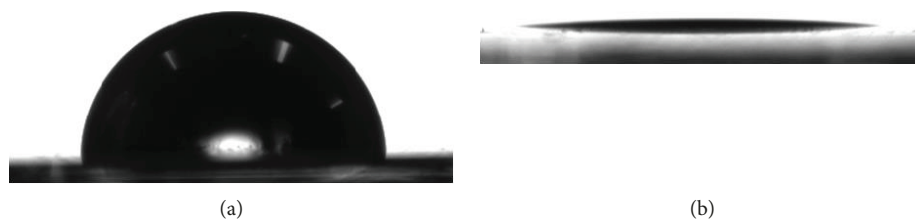


FIGURE 11: Contact angle measurements of a chemically reduced graphene oxide film with (a) deionized water and (b) chloroform.

the step in the yellow line in Figure 11(a). The step measurement was done through the profile shown in Figure 11(b), where the red line represents a height of approximately 16 nm.

There are different reasons, such as instrumental displacement and morphological properties of graphene sheets (folds and wrinkles), why, generally, steps with heights smaller than 1 nm are considered a single-layer graphene in AFM studies [48].

**3.7. Confocal Microscopy.** Confocal microscopy was used to calculate the thickness of the films. Table 2 shows the thicknesses of the GO and RGO samples. Thermally reduced films are quite rough and uneven, so they do not have the same thickness throughout the film area.

The thickness of GO films depends very much on the processing method. In the literature, there are reports of graphene oxide films with very varied thicknesses. For example, Nikolakopoulou et al. [10] produced GO films of about 60 mg with a thickness of 4  $\mu\text{m}$  by the deposition of 4 mL of a graphene oxide solution with a concentration of 15 mg/mL on a 1  $\times$  1 cm glass substrate. Meanwhile, Singh et al. in 2015 produced GO films with a thickness of 70 nm and 0.002 mg, by depositing 20  $\mu\text{L}$  of a solution of 0.1 mg/mL graphene oxide on a 1  $\times$  1 cm quartz substrate [10, 49]. GO films reduced with hydrazine were also produced by Yang and Zou [50] using a method similar to that used in this work. A solution of 0.25 mg/mL was used for the production of the films, with the thickness varying from 317 nm (5 mg of reduced GO) to 1300 nm (25 mg of reduced GO).

**3.8. Contact Angle Measurements.** The measured contact angles for the GO and RGO films produced in this work, with water and chloroform, are described in Table 3.

The equilibrium state of a graphene surface exposed to environmental conditions is of fundamental importance for the understanding of their behavior in practical applications. The level of wetting of the surface (its nature hydrophobic or hydrophilic) affects the graphene's properties, such as adhesion, gap, and mobility of ions [33].

The GOF presented an average contact angle of about 39°, that is, a hydrophilic behavior. Few studies are found in the literature reporting contact angle measurements for graphene and/or graphene oxide films, but it was possible to find angle values varying from 45.1 to 67.4° for GO films in contact with water [38, 39]. Considering that the higher the number of oxygen groups present, the greater the interaction of the GO film with water, and consequently, the lower the contact angle between them, this indicates the presence of a smaller number of functional groups, i.e., a

TABLE 2: Thickness of GO films.

Sample	Thickness (nm)
GOF	454
CGOF	130
TGOF	2131

TABLE 3: Contact angles.

Sample	Deionized water	Chloroform
GOF	38.9 $\pm$ 0.2	4.7 $\pm$ 0.5
TGOF	84.7 $\pm$ 3.5	~0
CGOF	90.6 $\pm$ 2.2	3.7 $\pm$ 0.3

TABLE 4: Surface tensions of GO and RGO films.

Sample	$\gamma_s^p$ (mJ/m <sup>2</sup> )	$\gamma_s^d$ (mJ/m <sup>2</sup> )	$\gamma_s$ (mJ/m <sup>2</sup> )
GOF	31.1	27.3	59.2 $\pm$ 0.1
TGOF	6.2	27.5	32.1 $\pm$ 1.3
CGOF	2.6	27.5	30.1 $\pm$ 0.6

graphite oxidation to a lesser degree than the GOF produced in this work. Moreover, the presence of these oxygenated groups increases the polarity of the film surface as well as its surface energy.

A contact angle with water of about 85° was obtained for the thermally reduced GO films (TGOF). It is much less hydrophilic than the initial GO film, indicating the efficient GO reduction. Wan et al. [37] obtained a contact angle with water of 67.3° for thermally reduced GO films. In this work, a higher average contact angle was obtained, which suggests a more efficient thermal reduction. Nevertheless, the rougher surface observed on the thermally reduced films in this work, according to the Wenzel model, can enhance the hydrophobicity of the samples [34, 35].

The chemically reduced GO film with sodium borohydride, CGOF, formed a contact angle with the water of approximately 90.6°, denoting a hydrophobic behavior. This lower level of interaction with the water gives also an indication of an efficient GO reduction. These results are similar to those found by Wan et al. [37] for a reduced GO film with molten aluminum (90.5°) and by Shin et al. [38] who obtained graphene films by epitaxial growth on a

silicon substrate ( $92.5^\circ$ ) and by orderly pyrolytic cleavage of graphite ( $91^\circ$ ).

The contact angles between the GO and RGO films and chloroform were much smaller if compared to the contact angles with water, due to the low polarity of chloroform. For the TGOF, it was not possible to measure the contact angle with respect to chloroform, because it was too small.

Figure 11 shows images obtained for the CGOF sample by measuring its contact angle with water and chloroform.

**3.9. Surface Tensions.** From the contact angles with water and chloroform, it was possible to calculate the surface tensions of the produced films. The results of the surface tensions are summarized in Table 4.

For the GO film (GOF), a surface tension of  $59.2 \text{ mJ/m}^2$  was obtained. Values very close to this were also found for GO films by Wang et al. [40] ( $62.1 \text{ mJ/m}^2$ ), Wan et al. [37] ( $54.8 \text{ mJ/m}^2$ ), and Konios et al. [39] ( $62 \text{ mJ/m}^2$ ). For the RGO films, smaller surface tensions were found, from  $32.1 \text{ mJ/m}^2$  for the TGOF to  $30.1 \text{ mJ/m}^2$  for the CGOF. In the literature, values of 46, 46.7, 39.2, and  $23.4 \text{ mJ/m}^2$  have been reported for RGO films [39, 40].

The existence of oxygen groups on the surface of the GO films results in a higher amount of energy at the surface of the material and consequently higher surface tension. In the reduced GO films, there is a loss of the polarity of the surface due to the elimination of a part of the oxygen groups present in the material because of the reduction, which increases its hydrophobicity; that is, it decreases its energy on the surface, resulting in lower values of superficial tension. This indicates that unreduced GO films have better adhesion than RGO films [39, 40].

## 4. Conclusions

Self-standing films of graphene oxide and reduced graphene oxide were produced from graphite by a low-cost vacuum filtration method and thoroughly characterized. The results show an efficient production of hydrophilic GO films and hydrophobic RGO films, by both chemical reduction with  $\text{NaBH}_4$  and thermal reduction at  $800^\circ\text{C}$  under argon.

However, XRD analyses of films produced by vacuum filtration revealed peaks not yet reported in the literature (corresponding to interplanar distances of 0.63 nm, 0.52 nm, and 0.48 nm), indicating that these films have a distinct crystalline structure. The films produced in this work probably present the combination of crystalline regions with different interplanar distances, which can be explained by the presence of graphene/graphene oxide intercalated sheets. As powder graphene oxide did not present these peaks, the formation of this unexpected crystalline structure is attributed to the vacuum filtration method.

## Data Availability

The raw data of all figures and tables included in the article are available from the corresponding author: sergio.pezzin@udesc.br.

## Conflicts of Interest

The authors declare that there is no conflict of interest regarding the publication of this paper.

## Acknowledgments

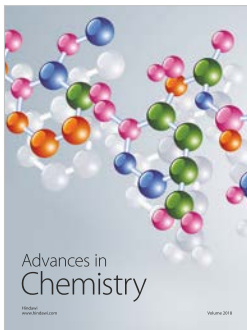
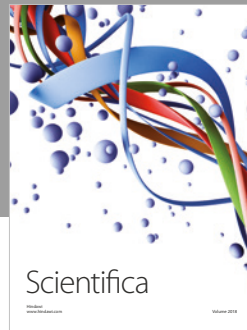
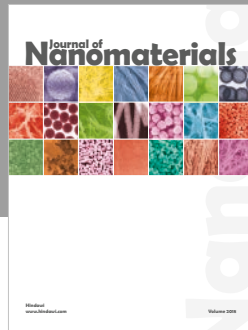
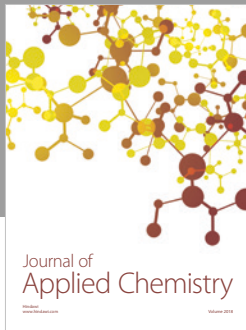
The authors would like to thank Prof. Masahiro Tomiyama (UDESC, Brazil) for the confirmatory XRD measurements and Prof. Dr. Monica de Mesquita Lacerda (UFRJ, Brazil) for the fruitful discussions. This research was funded by CAPES (Coordination of Improvement of Higher Level Personnel, Brazil), UDESC (Universidade do Estado de Santa Catarina), and FAPESC (Foundation for Research and Innovation Support of the State of Santa Catarina) (2015TR660).

## References

- [1] A. H. Castro Neto, F. Guinea, N. M. R. Peres, K. S. Novoselov, and A. K. Geim, "The electronic properties of graphene," *Reviews of Modern Physics*, vol. 81, no. 1, pp. 109–162, 2009.
- [2] C. Zhou, S. Chen, J. Lou et al., "Graphene's cousin: the present and future of graphane," *Nanoscale Research Letters*, vol. 9, no. 1, p. 26, 2014.
- [3] W. S. Hummers Jr and R. E. Offeman, "Preparation of graphitic oxide," *Journal of the American Chemical Society*, vol. 80, no. 6, p. 1339, 1958.
- [4] S. Park and R. S. Ruoff, "Chemical methods for the production of graphenes," *Nature Nanotechnology*, vol. 4, no. 4, pp. 217–224, 2009.
- [5] A. Geim and A. C. Neto, "Graphene," *New Scientist*, vol. 214, p. 2863, 2012.
- [6] A. A. Arbuzov, V. E. Muradyan, and B. P. Tarasov, "Synthesis of graphene-like materials by graphite oxide reduction," *Russian Chemical Bulletin*, vol. 62, no. 9, pp. 1962–1966, 2013.
- [7] H. A. Becerril, J. Mao, Z. Liu, R. M. Stoltenberg, Z. Bao, and Y. Chen, "Evaluation of solution-processed reduced graphene oxide films as transparent conductors," *ACS Nano*, vol. 2, no. 3, pp. 463–470, 2008.
- [8] S. Rapino, E. Treossi, V. Palermo, M. Marcaccio, F. Paolucci, and F. Zerbetto, "Playing peekaboo with graphene oxide: a scanning electrochemical microscopy investigation," *Chemical Communications*, vol. 50, no. 86, pp. 13117–13120, 2014.
- [9] M. J. McAllister, J.-L. Li, D. H. Adamson et al., "Single sheet functionalized graphene by oxidation and thermal expansion of graphite," *Chemistry of Materials*, vol. 19, no. 18, pp. 4396–4404, 2007.
- [10] A. Nikolakopoulou, D. Tasis, L. Sygellou, V. Dracopoulos, C. Galiotis, and P. Lianos, "Study of the thermal reduction of graphene oxide and of its application as electrocatalyst in quasi-solid state dye-sensitized solar cells in combination with PEDOT," *Electrochimica Acta*, vol. 111, pp. 698–706, 2013.
- [11] X. Yu, W. Zhang, P. Zhang, and Z. Su, "Fabrication technologies and sensing applications of graphene-based composite films: advances and challenges," *Biosensors and Bioelectronics*, vol. 89, Part 1, pp. 72–84, 2017.
- [12] S. Pei, J. Zhao, J. Du, W. Ren, and H.-M. Cheng, "Direct reduction of graphene oxide films into highly conductive and flexible graphene films by hydrohalic acids," *Carbon*, vol. 48, no. 15, pp. 4466–4474, 2010.

- [13] Q. Zheng, B. Zhang, X. Lin et al., "Highly transparent and conducting ultralarge graphene oxide/single-walled carbon nanotube hybrid films produced by Langmuir–Blodgett assembly," *Journal of Materials Chemistry*, vol. 22, no. 48, pp. 25072–25082, 2012.
- [14] A. Nekahi, P. H. Marashi, and D. Haghshenas, "Transparent conductive thin film of ultra large reduced graphene oxide monolayers," *Applied Surface Science*, vol. 295, pp. 59–65, 2014.
- [15] F. Han, S. Yang, W. Jing et al., "A highly efficient synthetic process of graphene films with tunable optical properties," *Applied Surface Science*, vol. 314, pp. 71–77, 2014.
- [16] V. H. Pham, T. V. Cuong, S. H. Hur et al., "Fast and simple fabrication of a large transparent chemically-converted graphene film by spray-coating," *Carbon*, vol. 48, no. 7, pp. 1945–1951, 2010.
- [17] H.-J. Shin, K. K. Kim, A. Benayad et al., "Efficient reduction of graphite oxide by sodium borohydride and its effect on electrical conductance," *Advanced Functional Materials*, vol. 19, no. 12, pp. 1987–1992, 2009.
- [18] A. Guimont, E. Beyou, P. Cassagnau et al., "Grafting of polyethylene onto graphite oxide sheets: a comparison of two routes," *Polymer Chemistry*, vol. 4, no. 9, p. 2828, 2013.
- [19] M. Brahmayya, S. A. Dai, and S.-Y. Suen, "Sulfonated reduced graphene oxide catalyzed cyclization of hydrazides and carbon dioxide to 1,3,4-oxadiazoles under sonication," *Scientific Reports*, vol. 7, no. 1, p. 4675, 2017.
- [20] M. Hiramatsu, H. Kondo, and M. Hori, "Graphene nanowalls," in *New Progress on Graphene Research*, J. R. Gong, Ed., InTech, 2013.
- [21] Y. Lu, T. Wang, Z. Tian, and Q. Ye, "Preparation of graphene oxide paper as an electrode for lithium-ion batteries based on a vacuum filtration method," *International Journal of Electrochemical Science*, vol. 12, pp. 8944–8952, 2017.
- [22] M. Hirata, T. Gotou, S. Horiuchi, M. Fujiwara, and M. Ohba, "Thin-film particles of graphite oxide 1: high-yield synthesis and flexibility of the particles," *Carbon*, vol. 42, no. 14, pp. 2929–2937, 2004.
- [23] K. Lau, M. Lu, H. Cheung, F. Sheng, and H. Li, "Thermal and mechanical properties of single-walled carbon nanotube bundle-reinforced epoxy nanocomposites: the role of solvent for nanotube dispersion," *Composites Science and Technology*, vol. 65, no. 5, pp. 719–725, 2005.
- [24] Z. Lin, Y. Yao, Z. Li, Y. Liu, Z. Li, and C. P. Wong, "Solvent-assisted thermal reduction of graphite oxide," *Journal of Physical Chemistry C*, vol. 114, no. 35, pp. 14819–14825, 2010.
- [25] S. Peng, X. Fan, S. Li, and J. Zhang, "Green synthesis and characterization of graphite oxide by orthogonal experiment," *Journal of the Chilean Chemical Society*, vol. 58, no. 4, pp. 2213–2217, 2013.
- [26] Z. Q. Li, C. J. Lu, Z. P. Xia, Y. Zhou, and Z. Luo, "X-ray diffraction patterns of graphite and turbostratic carbon," *Carbon*, vol. 45, no. 8, pp. 1686–1695, 2007.
- [27] K. H. Kim, M. Yang, K. M. Cho, Y. S. Jun, S. B. Lee, and H. T. Jung, "High quality reduced graphene oxide through repairing with multi-layered graphene ball nanostructures," *Scientific Reports*, vol. 3, no. 1, p. 3251, 2013.
- [28] Q. Ke and J. Wang, "Graphene-based materials for supercapacitor electrodes — a review," *Journal of Materiomics*, vol. 2, no. 1, pp. 37–54, 2016.
- [29] X. Jiao, Q. Hao, X. Xia et al., "Free-standing hybrid graphene paper encapsulating nanostructures for high cycle-life supercapacitors," *ChemSusChem*, vol. 11, no. 5, pp. 907–915, 2018.
- [30] K. Zhang, Y. Zhang, and S. Wang, "Enhancing thermoelectric properties of organic composites through hierarchical nanostructures," *Scientific Reports*, vol. 3, no. 1, p. 3448, 2013.
- [31] M. Acik, G. Lee, C. Mattevi et al., "The role of oxygen during thermal reduction of graphene oxide studied by infrared absorption spectroscopy," *Journal of Physical Chemistry C*, vol. 115, no. 40, pp. 19761–19781, 2011.
- [32] F. C. Fim, *Síntese e Propriedades de Nanocompósitos de Polietileno/Nanolâminas de Grafeno Obtidos Através de Polimerização In Situ 2012*, [PhD Thesis], (Materials Science) – Universidade Federal do Rio Grande do Sul, Porto Alegre, 2012.
- [33] M. Khenfouch, M. Baïtoul, H. Aarab, and M. Maaza, "Morphological, vibrational and thermal properties of confined graphene nanosheets in an individual polymeric nanochannel by electrospinning," *Graphene*, vol. 1, no. 2, pp. 15–20, 2012.
- [34] Z. Tang, L. Zhang, C. Zeng, T. Lin, and B. Guo, "General route to graphene with liquid-like behavior by non-covalent modification," *Soft Matter*, vol. 8, no. 35, pp. 9214–9220, 2012.
- [35] M. Naebe, J. Wang, A. Amini et al., "Mechanical property and structure of covalent functionalised graphene/epoxy nanocomposites," *Scientific Reports*, vol. 4, no. 1, 2014.
- [36] M. Boota, K. B. Hatzell, M. Alhabeab, E. C. Kumbur, and Y. Gogotsi, "Graphene-containing flowable electrodes for capacitive energy storage," *Carbon*, vol. 92, pp. 142–149, 2015.
- [37] D. Wan, C. Yang, T. Lin et al., "Low-temperature aluminum reduction of graphene oxide, electrical properties, surface wettability, and energy storage applications," *ACS Nano*, vol. 6, no. 10, pp. 9068–9078, 2012.
- [38] Y. J. Shin, Y. Wang, H. Huang et al., "Surface-energy engineering of graphene," *Langmuir*, vol. 26, no. 6, pp. 3798–3802, 2010.
- [39] D. Konios, M. M. Stylianakis, E. Stratakis, and E. Kymakis, "Dispersion behaviour of graphene oxide and reduced graphene oxide," *Journal of Colloid and Interface Science*, vol. 430, pp. 108–112, 2014.
- [40] X. Wang, L. Zhi, and K. Mullen, "Transparent, conductive graphene electrodes for dye-sensitized solar cells," *Nano Letters*, vol. 8, no. 1, pp. 323–327, 2008.
- [41] X. Feng, W. Chen, and L. Yan, "Free-standing dried foam films of graphene oxide for humidity sensing," *Sensors and Actuators B*, vol. 215, pp. 316–322, 2015.
- [42] C. Bora, C. Sarkar, K. J. Mohan, and S. Dolui, "Polythiophene/graphene composite as a highly efficient platinum-free counter electrode in dye-sensitized solar cells," *Electrochimica Acta*, vol. 157, pp. 225–231, 2015.
- [43] S. Hun, "Thermal reduction of graphene oxide," in *Physics and Applications of Graphene — Experiments*, S. Mikhailov, Ed., 2011.
- [44] S. Wu, X. Zhao, Y. Li et al., "Adsorption properties of doxorubicin hydrochloride onto graphene oxide: equilibrium, kinetic and thermodynamic studies," *Materials*, vol. 6, no. 5, pp. 2026–2042, 2013.
- [45] S. Abdolhosseinzadeh, H. Asgharzadeh, and H. Seop Kim, "Fast and fully-scalable synthesis of reduced graphene oxide," *Scientific Reports*, vol. 5, no. 1, 2015.

- [46] N. R. Wilson, P. A. Pandey, R. Beanland et al., "Graphene oxide: structural analysis and application as a highly transparent support for electron microscopy," *ACS Nano*, vol. 3, no. 9, pp. 2547–2556, 2009.
- [47] R. Hack, C. H. G. Correia, R. A. de Simone Zanon, and S. H. Pezzin, "Characterization of graphene nanosheets obtained by a modified Hummer's method," *Matéria (Rio de Janeiro)*, vol. 23, no. 1, 2018.
- [48] A. Hadi, J. Zahirifar, J. Karimi-Sabet, and A. Dastbaz, "Graphene nanosheets preparation using magnetic nanoparticle assisted liquid phase exfoliation of graphite: the coupled effect of ultrasound and wedging nanoparticles," *Ultrasonics Sonochemistry*, vol. 44, pp. 204–214, 2018.
- [49] M. Singh, A. Yadav, S. Kumar, and P. Agarwal, "Annealing induced electrical conduction and band gap variation in thermally reduced graphene oxide films with different  $sp^2/sp^3$  fraction," *Applied Surface Science*, vol. 326, pp. 236–242, 2015.
- [50] J. Yang and L. Zou, "Graphene films of controllable thickness as binder-free electrodes for high performance supercapacitors," *Electrochimica Acta*, vol. 130, pp. 791–799, 2014.



**Hindawi**  
Submit your manuscripts at  
[www.hindawi.com](http://www.hindawi.com)

